Vol. 91 No. 6 pp. 2126–2137 ACTA GEOLOGICA SINICA (English Edition) Dec. 2017

Genesis and Uranium Sources of Leucogranite-hosted Uranium Deposits in the Gaudeanmus Area, Central Damara Belt, Namibia: Study of Element and Nd Isotope Geochemistry

FAN Honghai[1, 2, 3, *], CHEN Jinyong[1, 2], WANG Shengyun[1, 2], ZHAO Jingyang[1, 2], GU Dazhao[1, 2] and MENG Yanning[1, 2]

1 *Beijing Research Institute of Uranium Geology, Beijing 100029, China*

2 *Key Laboratory of Uranium Resource Exploration and Evaluation Technology, CNNC, Beijing 100029, China*

3 *Department of Earth Sciences and State Key Lab of Mineral Deposit Research, Nanjing University, Nanjing 210093, China*

Abstract: This paper presents a systematic study of major and trace elements and Sm-Nd isotopes in leucogranites closely related to uranium mineralization in the Gaudeanmus area, Namibia. The results illustrate that the uraniferous leucogranites possess high SiO_2 (68.8wt%–76.0wt%, average 73.1wt%) and K (4.05wt%–7.78wt%, average 5.94wt%) contents, and are sub-alkaline and metaluminous to weakly peraluminous, as reflected by A/CNK values of 0.96–1.07 with an average of 1.01. The leucogranites are rich in light rare earth elements (LREE/HREE = 2.53–7.71; $(La/Yb)_N$ = 2.14–10.40), have moderate Eu depletion and high Rb/Sr ratios (2.03–5.50 with an average of 4.36); meanwhile, they are enriched in Rb, K, Th, U and Pb, and depleted in Ba, Nb, Ta, and Sr. The $\varepsilon_{Nd}(t)$ values of uraninites range from −14.8 to −16.5, and the two-stage Nd model ages are 2.43–2.56 Ga. Detailed elemental and Sm-Nd isotopic geochemical characteristics suggest that the leucogranites were formed in a post-orogenic extensional environment. The U-rich pre-Damara basement was the main source of uranium during the primary mineralization event, which is disseminated in leucogranites, whereas the uranium mineralization in veins possibly resulted from remobilization of the primary uranium minerals.

Key words: uranium, source of uranium, Nd isotopes, leucogranites, Gaudeanmus, Damara Belt

1 Introduction

Namibia hosts abundant uranium resources, which have been grouped into three types according to their lithological setting. These include: a) occurrences associated with plutonic rocks, b) sedimentary occurrences and c) pedogenic occurrences (Roesener and Schreuder, 1994). The world-class Rössing deposit in Namibia typifies the leucogranite-hosted uranium deposits (Cuney, 1980a). The Rössing Uranium Mine, situated approximately 60 km NE of Swakopmund, Namibia, is the only economic leucogranite-hosted uranium deposit being exploited at present. The Paleozoic Rössing deposit is, by virtue of its age, host rocks, size, grade and U-Th ratio that yields extremely low radioactivity, exceptional in both African and global contexts (Barnes and Hambleton-Jones, 1978). The Rössing deposit also typifies the ‘‘intrusive-alaskite’’ types. In keeping with recent developments, the term ‘‘leucogranite-hosted’’ is used here, rather than ‘‘intrusive-alaskite’’ or ‘‘alaskite-hosted’’, allowing a more generic overview of the leucogranites of the Central Zone of the Damara Orogen.

Several uranium occurrences and deposits have been found in the Gaudeanmus area near the Rössing deposit, including one located about 3.5km southeast of the Rössing deposit (Fig.1). Recent studies of the mineralizing fluids and uranium mineralogy in uraniferous leucogranites of the Gaudeanmus area (Chen et al., 2013 and 2014; Fan et al., 2015; Zong et al., 2015), and at the Rössing, Rössing South, and Ida Dome deposits (Cuney, 1980a and 1980b; Nex et al., 2001, 2002; Basson et al., 2004; Kinnaird et al., 2007; Corvino and Pretorius, 2013), have shed some light on the mineralizing processes.

* Corresponding author. E-mail: fhh270@263.net

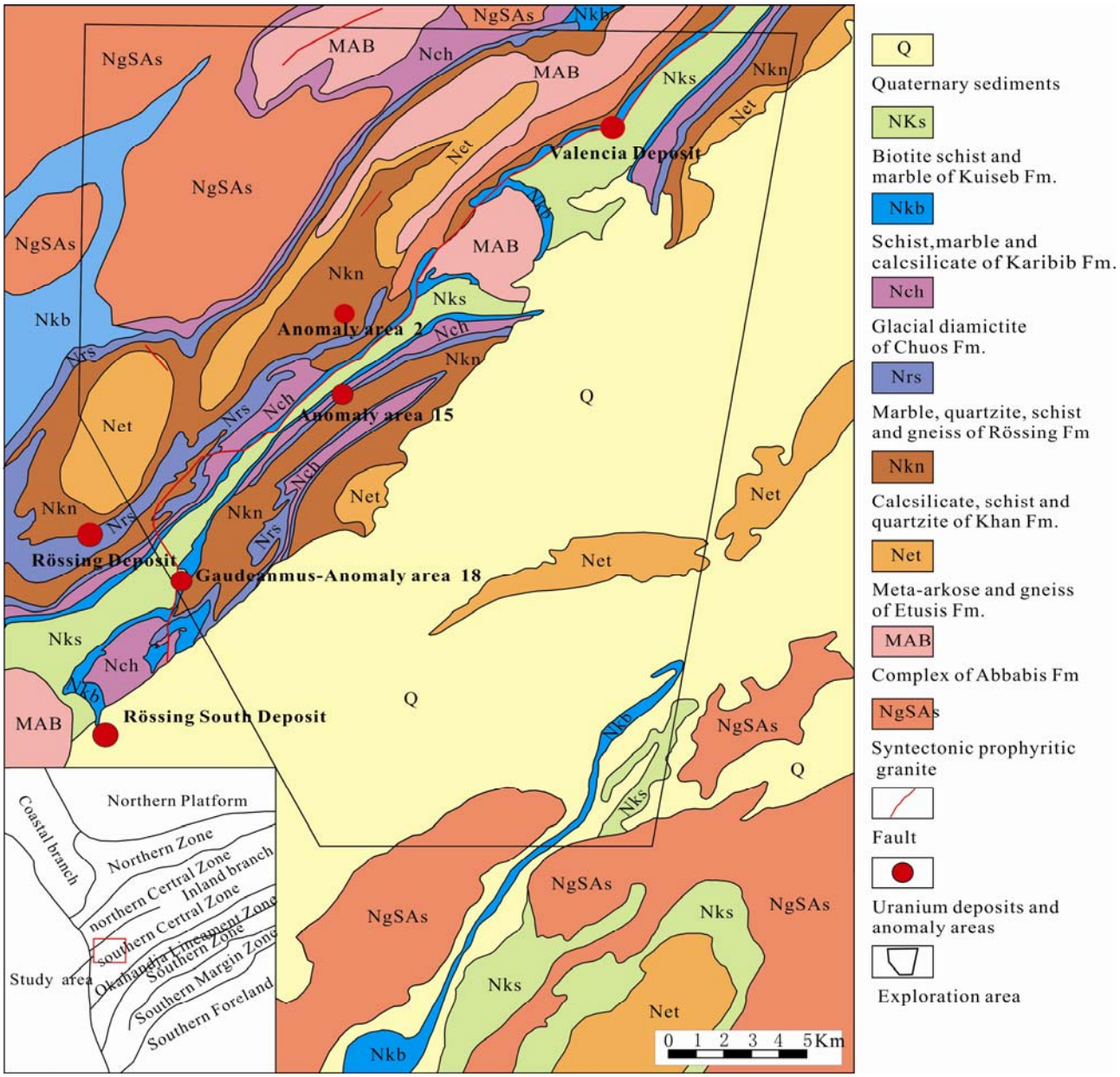

Fig. 1. Geological map of the Gaudeanmus area, Namibia, showing the location of significant uranium anomalies (inset map shows location relative to structural domains of southwestern Africa; after Chen et al., 2013).

However, the uranium genesis and the sources of the mineralized fluids are still in debate. There are four theories: 1) based on their compositions and setting along the boundary between the Khan and Rössing Formation, Smith (1965) suggested that the uraniferous leucogranites originated from uraniferous protosediments during amphibolite-facies metamorphism; 2) Barnes and Hambleton-Jones (1978) interpreted oxidation halos observed in the leucogranite as cryptic enclaves of Khan Formation meta-sediments, leading them to suggest the Khan Formation as the source for the uranium mineralization; 3) Jacob (1978), Haack et al. (1983), and Nex et al. (2001) showed that the pre-Damaran basement rocks are anomalously radioactive and can therefore provide an alternate source of uranium, and 4) Brynard and Andreoli (1988) proposed that the uraniferous leucogranites were derived by remelting of high-heat producing (HHP) red granite. This paper presents the results of a systematic study on the geochemistry of uraniferous leucogranites and Sm-Nd systematics of uraninites within uraniferous leucogranites. It also addresses the uranium genesis of uraniferous leucogranites in the Gaudeanmus area.

2 Geological Setting

Across the African continent, the Neoproterozoic to early Paleozoic (650–460 Ma) Damara Belt constitutes

part of the Pan-African Mobile Belt, which resulted from continental collision of the Congo and Kalahari cratons (Coward, 1983). In Namibia it consists of two main branches, the N-trending coastal branch and the NW-trending intracontinental inland branch. The inland branch is further subdivided into several structural domains, including Northern Platform, Northern Zone, Central Zone (further subdivided into northern and southern), Okahandja Lineament Zone, Southern Zone, Southern Marginal Zone, and Southern Foreland (Fig. 1; Martin et al., 1977; Kitt, 2008). The boundaries of each domain were defined by interpreted regional aeromagnetic structures or lineaments (Corner, 1983). All of the leucogranite-hosted uranium occurrences in Namibia are situated in the Central Zone (Fig.2; Roesener and Schreuder, 1994). The Gaudeanmus area lies in the southern Central Zone (Fig. 1), which is characterized by voluminous granitic intrusions and a regional amphibolite to granulite-facies metamorphic event (Miller, 1983).

In the Gaudeanmus area, the pre-Damara basement gneisses (~2 Ga) are unconformably overlain by the Neoproterozoic Damara sequence which comprises the Nosib Group and the Swakop Group. The Nosib Group has been divided into the Etusis and Khan formations. The overlying Swakop Group comprises the Rössing, Chuos, Karibib, and Kuiseb formations (Table 1). Uraniferous leucogranites occur as veins intrude into the Rössing and Khan formations, or the Karibib and Kuiseb formations (in cases where the Rossing Formation is thin or absent).

3 Leucogranite Petrology

The Central Zone of Damara Belt is renowned for the emplacement of voluminous intrusions, covering an exposed area of at least 75,000 km^2. Among over 300 intrusive bodies, 96% are granites, with the rest being of mafic rocks, diorite, and granodiorite (Miller, 1983). The granites are subdivided into four suites, as described in Miller (1983), including the Salem Suite, the Red gneissic granites, the equigranular-textured Grey Granites and the sheeted leucogranites. The Salem suite includes porphyritic granite (552.5±2.2 Ma, LA-ICP-MS U-Pb zircon) and biotite granite (540.2±3.9 Ma, LA-ICP-MS U-Pb zircon), and contains abundant garnet (Wang, 2013). The ages of the red gneissic granite and grey granite are 535.6±7.2 Ma (SHRIMP U-Pb monazite) and 520.4±4.2

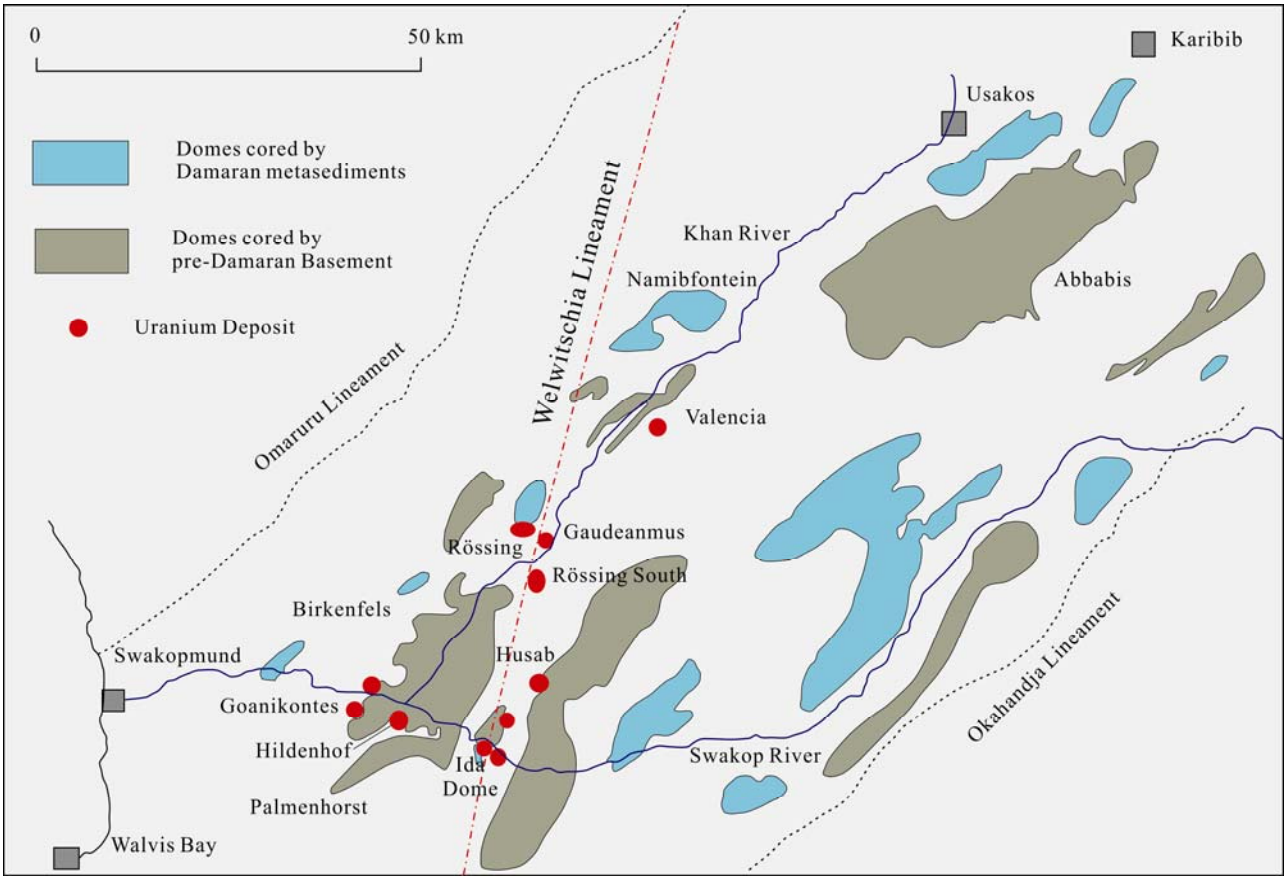

Fig. 2. Map showing distribution of various domes, the Welwitschia Lineament and spatially associated primary uranium deposits of the Central Zone (based on data from Corner, 1983; Anderson and Nash, 1997; Basson and Greenway, 2004; and Kinnaird and Nex, 2007).

Table 1 Stratigraphic succession of Central Damara Belt in Gaudeanmusarea, Namibia (after Smith, 1965; Nex, 1997)

Group	Subgroup	Formation	Maximum thickness	Lithology	Age
Swakop	Khomas	Kuiseb	>3000m	Pelitic and semi-pelitic schist and gneiss, migmatite, calc-silicate rock, quartzite.	～710 Ma（Hoffmann et al.，2004）
		Karibib	1000m	Marble, calc-silicate rock, pelitic and semi-pelitic schist and gneiss, biotite amphibolite schist, quartz schist, migmatite.	
		Chuos	700m	Diamictite, calc-silicate rock, pebbly schist, quartzite, ferruginous quartzite, migmatite.	
	Discordance				
	Ugab	Rössing	200m	Marble, pelitic schist and gneiss, biotite-hornblende schist, migmatite, calc-silicate rock, quartzite, metaconglomerate.	
	Discordance				
Nosib		Khan	1100m	Migmatite, banded and mottled quartzofelds-pathicclinopyroxene-amphibolite gneiss, hornblende-biotite schist, biotite schist and gneiss, migmatite, pyroxene-garnet gneiss, amphibolite, quartzite, metaconglomerate.	
		Etusis	3000m	Quartzite, metaconglomerate, pelitic and semi-pelitic schist and gneiss, migmatite, quartzofelds-pathicclinopyroxene-amphibolite gneiss, calc-silicate rock, metarhyolite.	
Major unconformity					
Abbabis Complex				Gneissic granite, augen gneiss, quartzofelds-pathic gneiss, pelitic schist and gneiss, migmatite, quartzite, marble, calc-silicate rock, amphibolite.	～2 Ga（Longridge et al., 2008）

Ma (SHRIMP U-Pb zircon), respectively (Longridge, 2011).

The sheeted leucogranite can be grouped into six distinct types (presented in Table 2) based on observable field characteristics of structural setting, form of intrusion, colour, grain size, texture, radioactivity and macro-scale mineralogy (Nex, 1997). Only D and E-type leucogranites are uranium-bearing. D-type leucogranites dominate the study area, with few E-type leucogranite outcrops, the and E-type leucogranites are a product of variably influenced metasomatic alteration of the D-type (Freemantle, 2010).

4 Uranium Mineralogy

On the basis of thin-section microscopic observation and electron-probe analysis, it is shown that uranium in the leucogranites mainly occurs as independent uranium minerals, with minor amounts substituting for thorium in thorium-bearing accessory minerals. Uranium minerals chiefly consist of uranium oxides, uranium-titanium oxides, and uranium silicates, and commonly coexist with zircon, apatite, monazite, pyrite, molybdenite, galena, and sphalerite (Fig. 3a). Uranium oxides comprise uraninite, pitchblende, and broggerite. Uraninite is crystallized during fractional crystallization of the leucogranite magma, and is characterized by large grain sizes around 0.1–0.05 mm (Fig. 3b). Occasionally these grains reside within rock-forming minerals (e.g. plagioclase and biotite) and the contacts between uraninite and host minerals tend to generate radioactive halos. In contrast, pitchblende is present as veins or veinlets (Fig. 3c), which are inferred to have formed during a post-magmatic hydrothermal overprint. Uranium-titanium oxides include a group of complex minerals, such as brannerite, betafite, and uranpyrochlore, which are also crystallized during fractional crystallization of the leucogranite magma. Uranium silicates include coffinite, uranothorite, and uranophane, the latter of which forms as a secondary uranium mineral (Fig. 3d), due to supergene leaching. The primary uranium minerals, such as uraninite, broggerite

Table 2 Characteristics of different types of leucogranites in the Gaudeanmus area, Namibia

Type	Diagnostic mineralogical features	Radioactivity	Age（Ma）	References
A	Thin, very light pink to white, bedding parallel, very little accessories, often folded and boudinaged within Damaran metasediments	low Th>U	547.4±3.6 (LA-ICP-MS U-Pb zircon)	Wang, 2013
B	White as well as light pink, medium grained and homogeneous often bedding parallel, folded and boudinaged. Garnet is a distinctive accessory and is found in clusters or as disseminated grains mostly < 1 cm in size	low Th>U	537.8±4.3 (LA-ICP-MS U-Pb zircon)	Wang, 2013
C	Pale pink-cream, medium-pegmatitic grain size, hypersolvus with interstitial clear quartz, magnetite, ilmenite and tourmaline	Low, high in patches, Th>U	525.4±2.6 (LA-ICP-MS U-Pb zircon)	Wang, 2013
D	White, medium-coarse grain size, granular texture, white feldspar with characteristic smoky quartz, frequently visible beta-uranophane and occasional betafite	very high U >Th	506±8.1(SHRIMP U-Pb zircon) 497±5.5 (LA-ICP-MS U-Pb zircon)	Longridge et al., 2008 Wang, 2013
E	Extremely variable colour and grain size, contains ‘‘oxidation haloes’’ (Corner and Henthorn, 1978)	High- very high U >Th	Age may be the same as D-typeleucogranite	Freemantle, 2010
F	Distinctive red colour, coarse-pegmatitic grain size, pink perthitic feldspar and milky coloured quartz	low U≈Th	511.4±4.3 (LA-ICP-MS U-Pb zircon)	Chen, 2014

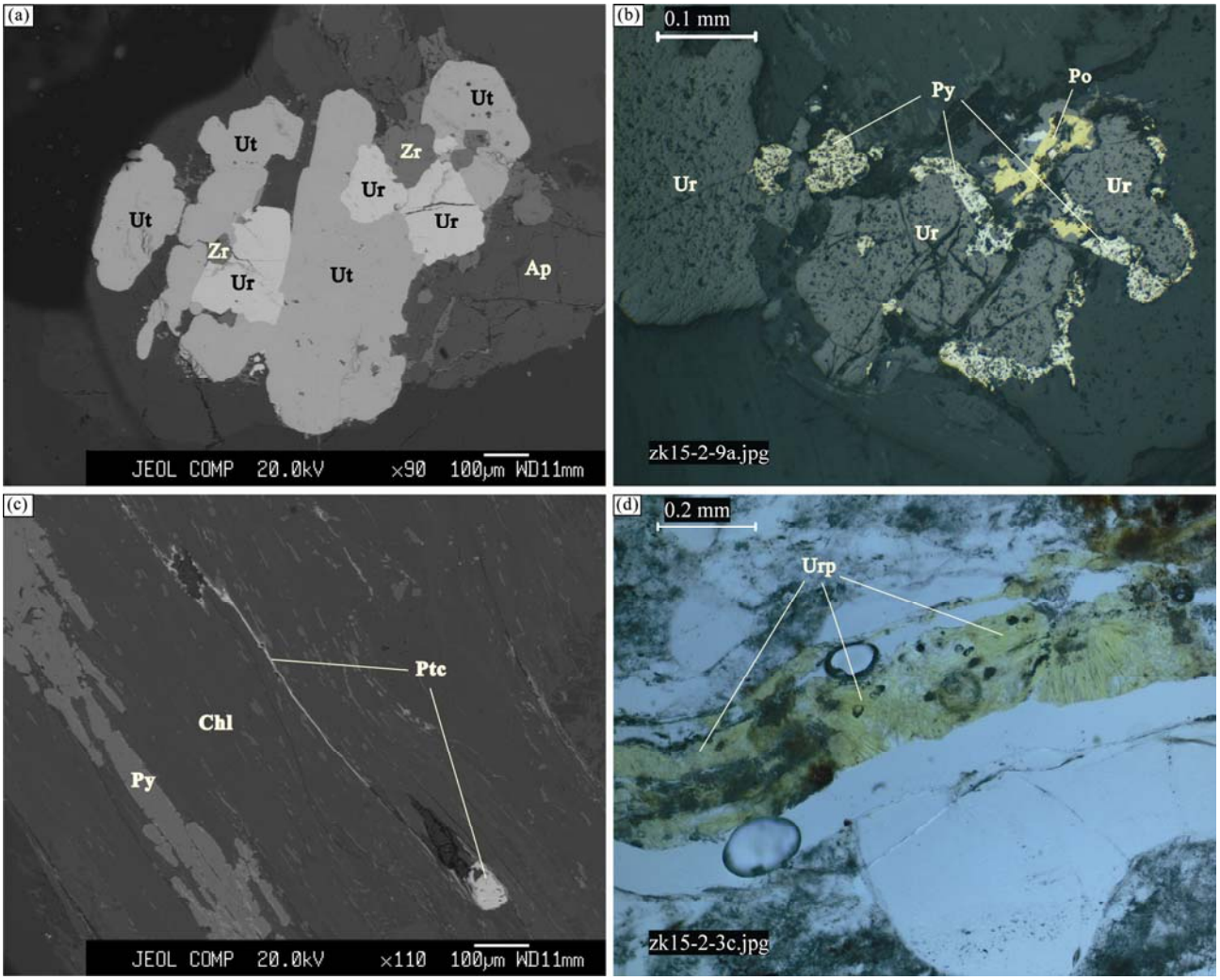

Fig. 3. Characteristics of uranium minerals in uraniferous leucogranites.
(a) Uraninite and uranothorite coexisting with zircon and apatite. (b) Hypidiomorphic granular uraninite partially mantled by pyrite. (c) Pitchblende vein filling a fracture in chlorite. (d) Vein of supergene mineralization displaying radial uranophane.

and brannerite, account for about 69% of the ore minerals, and the secondary uranium minerals, such as coffinite, uranothorite, pitchblende and uranophane, approximately account for 31%. Thus, the leucogranite-type uranium deposit in this area is a composite product of magmatic fractional crystallization, post-magmatic hydrothermal alteration, and supergene leaching (Chen et al., 2013).

5 Geochemical Characteristics

5.1 Analytical methods

All samples were collected in the No. 18 mineralization zone (Fig. 1). The detailed description of samples is presented in Table 3.

Compositional analyses for whole-rock major and trace elements were conducted at the Analytical Laboratory, Beijing Research Institute of Uranium Geology. Major element compositions were determined using a Philips PW2404 X-ray fluorescence spectrometer (XRF), with analytical precision better than 1%; FeO was measured using the volumetric method. Trace elements were measured with a Finnigan-MAT Element I HR-ICP-MS. About 50 mg of powered sample was dissolved in high-pressure Teflon bombs using a HF + HNO_3 mixture. Rh was used as an internal standard to monitor signal drift during counting. Relative uncertainty is less than 5% when

Table 3 Sample description of leucogranite in the Gaudeanmus area, Namibia

Sample no.	X	Y	Depth (m)	Lithology
ZK76-13-2			288.42─288.56	D-type leucogranite
ZK76-13-4			292.46─292.6	D-type leucogranite
ZK76-13-7			300.22─300.3	D-type leucogranite
ZK76-13-8			300.45─300.5	D-type leucogranite
ZK76-13-9			300.74─300.88	D-type leucogranite
ZK76-13-10	7510880	508299	302.1─302.25	D-type leucogranite
ZK76-13-12			305.73─305.88	D-type leucogranite
ZK76-13-13			309.75─309.88	D-type leucogranite
ZK76-13-14			311.03─311.13	D-type leucogranite
ZK76-13-16			315.19─315.3	D-type leucogranite
ZK76-13-18			324.28─324.41	D-type leucogranite
ZK84-6-3	7510604	508101	264.16─264.4	D-type leucogranite
LS-2	7510229	509254		D-type leucogranite

concentrations of trace and rare earth elements are greater than 10 ppm, whereas is the uncertainty is less than 10% when the concentrations are lower than 10 ppm. Analytical procedures for trace and rare earth elements are described by Gao et al. (2003).

Nd isotopic analysis of uraninites was completed at the Analytical Laboratory, Beijing Research Institute of Uranium Geology, using the analytical procedures described by Zhang et al. (1999). The reported $^{143}Nd/^{144}Nd$ ratios were normalized to a $^{146}Nd/^{144}Nd$ ratio of 0.7219. The analytical result of standard JMC yielded 0.512109±3, and the blank of Sm and Nd for the entire analytical procedure was less than 50×10^{-12} (Ding et al., 2016; Zhang et al., 2017).

5.2 Major and trace element geochemistry

Seven uraniferous leucogranite samples from the Gaudeanmus area were analyzed for their major and trace element compositions, and the results are presented in Table 4. The uraniferous leucogranites possess high silica (68.8wt%–76.0wt%, averaging 73.1wt%) and total alkaline (K_2O+Na_2O 8.5wt%–11.8wt%, averaging 9.7wt%) concentrations, with Na_2O ranging from 1.5wt%–4.6wt%, and K_2O/Na_2O ratios of 1.06–5.71 (mainly over 1.5 indicating potassium-rich compositions); concentrations of MnO, TiO_2, and MgO are relatively low. On the TAS diagram (Irvine et al., 1971), all samples plot within the subalkaline domain (Fig. 4a). The A/CNK ratios range from 0.96 to 1.07, with an average of 1.01. On the A/NK-A/CNK diagram, the plotted sample points concentrate in the metaluminous and peraluminous domains (Fig.4b), implying that the uraniferous leucogranites belong to subalkaline metaluminous-peraluminous rocks.

Table 4 shows that the analyzed uraniferous leucogranites have total REE concentrations of 96.5 ppm to 695 ppm (average 264 ppm). On a chondrite-normalized plot, the LREE display greater enrichment than the HREE (Fig. 5a). The LREE define a strongly negative slope that flattens through the HREE, showing significant fractionation between LREE and HREE elements (LREE/HREE=2.53–7.71 (average 5.03); $(La/Yb)_N$=2.14–10.4, (average 5.85)). It also displays moderate Eu depletion (δEu=0.18–0.80，average 0.45), indicating that the uraniferous leucogranites may have formed from fractional crystallization.

Based on Table 4 and the trace-element spidergram (Fig. 5b), the uraniferous leucogranites are enriched in Rb, Th, U, K, and Pb, and depleted in Ba, Nb, Ta, and Sr, typical of the continental crust. Rb/Sr ratios range from 2.03 to 5.50 with an average of 4.36, far higher than the global average upper crustal average of 0.32 (Taylor and McLennan, 1995), indicating highly mature crustal material in the source areas of the leucogranites.

On the Rb-Y+Nb diagram proposed by Pearce (1996) to discriminate between different tectonic settings, the uraniferous leucogranites plot within an area overlapping post-COLG (post-collision granite), syn-COLG (syn-collision granite) and WPG (within plate granite) (Fig. 6a). However, on the SiO_2-Al_2O_3 diagram proposed by Maniar and Piccoli (1989), the leucogranites of this study plot in the field for post-orogenic granites (POG) (Fig. 6b). These diagrams further support the interpretation that the uraniferous leucogranites were formed in a post-orogenic extensional setting.

5.3 Nd isotopic characteristics of uraninites

To further study the genesis of the uranium

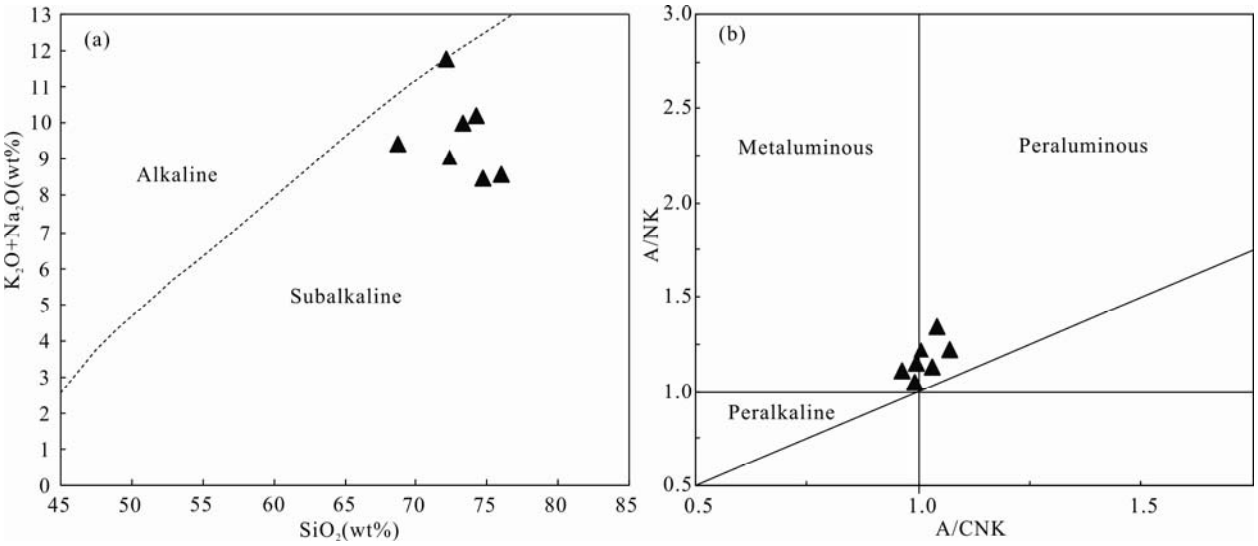

Fig. 4. Uraniferous leucogranites from the Gaudeanmus area, Namibia plotted on (a) TAS diagram (after Irvine et al., 1971) and (b) A/CNK-A/NK diagram.

Table 4 Major (wt%) and, trace and rare earth elements (ppm) concentrations of Uraniferous leucogranites in the Gaudeanmus area, Namibia

Sample	ZK76-13-2	ZK76-13-4	ZK76-13-7	ZK76-13-9	ZK76-13-13	ZK76-13-14	ZK76-13-18
SiO_2	72.39	72.16	74.81	73.31	76.02	74.25	68.81
TiO_2	0.26	0.03	0.20	0.07	0.04	0.07	0.08
Al_2O_3	13.66	14.75	12.84	13.10	12.43	13.45	17.11
$^{T}Fe_2O_3$	1.22	0.10	1.32	0.68	0.29	0.33	0.44
FeO	1.05	<0.10	1.15	0.25	0.15	0.15	0.15
MgO	0.59	0.10	0.53	0.20	0.17	0.16	0.27
CaO	1.33	0.41	0.81	0.99	0.94	0.65	2.00
MnO	0.02	0.01	0.02	0.01	0.01	0.01	0.01
Na_2O	2.43	2.45	2.35	1.77	2.62	1.52	4.59
K_2O	6.63	9.34	6.16	8.24	6.00	8.68	4.86
P_2O_5	0.35	0.07	0.07	0.37	0.12	0.16	0.34
LOI	0.98	0.59	0.90	1.12	1.23	0.61	1.49
Total	99.86	100.00	100.01	99.85	99.87	99.89	100.00
A/CNK	1.01	0.99	1.07	0.96	0.99	1.03	1.04
K_2O/Na_2O	2.73	3.81	2.62	4.66	2.29	5.71	1.06
Li	36.10	4.66	22.70	5.87	5.51	7.61	13.8
Be	2.69	1.72	2.32	1.75	3.10	1.37	10.3
Sc	6.20	1.98	5.45	3.14	2.64	3.14	3.72
V	39.9	3.88	30.2	9.05	5.92	12.1	8.84
Cr	1.66	0.50	1.10	0.70	0.59	0.85	0.88
Co	1.67	0.13	1.76	1.92	0.42	0.71	0.57
Ni	1.14	0.21	0.91	0.89	0.51	0.85	1.14
Cu	13.4	1.42	10.5	15.5	2.16	7.41	1.76
Zn	12.9	2.92	13.10	6.60	3.12	5.94	6.43
Ga	16.6	13.1	14.8	12.9	12.7	13.5	23.8
Rb	415	520	389	511	390	586	297
Sr	99.2	94.5	98.6	100	84.9	114	146
Y	120	23.8	53.3	57.9	37.5	47.1	83.0
Nb	28.3	3.25	25.0	11.4	6.77	11.2	11.5
Mo	1.60	0.72	7.24	1.19	4.84	1.22	57.7
Cd	0.03	0.02	0.06	0.01	0.02	0.03	0.02
In	0.02	0.00	0.02	0.01	0.01	0.01	0.01
Sb	1.23	0.39	1.23	1.58	0.68	0.99	5.54
Cs	4.90	6.78	5.03	5.84	8.74	6.24	7.00
Ba	408	556	322	480	322	507	228
Ta	1.82	0.49	1.85	1.18	1.31	1.13	1.48
W	1.30	0.46	1.18	1.95	1.10	1.79	0.84
Re	0.00	0.00	0.00	0.00	0.00	0.00	0.00
Tl	1.89	2.29	1.63	2.30	1.66	2.49	1.34
Pb	169.0	75.5	114.0	65.3	77.1	78.5	88.3
Bi	0.05	0.04	0.03	0.05	0.09	0.11	0.05
Th	325	70.0	130	88.2	69.0	104	137
U	1784	422	1209	37.2	627	524	744
Zr	349	119	970	176	420	443	806
Hf	10.6	3.86	30.0	5.46	12.9	13.7	25.4
Rb/Sr	4.18	5.50	3.95	5.11	4.59	5.14	2.03
La	144	34.1	30.1	19.4	16.7	50.1	74.5
Ce	285	63.5	60.7	43.0	32.9	94.8	143
Pr	34.0	6.89	7.12	5.36	3.78	10.9	16.7
Nd	120	23.2	26.4	21.3	13.8	38.4	60.3
Sm	25.3	4.68	6.88	6.15	3.79	8.53	13.6
Eu	1.40	1.17	0.91	0.99	0.84	1.09	1.02
Gd	21.6	4.05	6.86	6.63	4.15	7.44	12.2
Tb	4.54	0.85	1.70	1.70	1.08	1.57	2.60
Dy	27.1	5.22	11.20	11.40	7.15	9.54	16.2
Ho	5.09	1.00	2.33	2.39	1.50	1.95	3.24
Er	14.1	3.04	7.36	7.35	4.76	6.05	10.1
Tm	1.89	0.44	1.15	1.13	0.76	0.89	1.57
Yb	9.93	2.39	6.89	6.50	4.65	5.36	9.27
Lu	1.29	0.33	1.01	0.92	0.68	0.80	1.38
ΣREE	695.24	150.87	170.61	134.22	96.54	237.42	365.68
LREE	609.70	133.54	132.11	96.20	71.81	203.82	309.12
HREE	85.54	17.33	38.50	38.02	24.73	33.60	56.56
LREE/HREE	7.13	7.71	3.43	2.53	2.90	6.07	5.47
$(La/Yb)_N$	10.40	10.23	3.13	2.14	2.58	6.70	5.76
δEu	0.18	0.80	0.40	0.47	0.64	0.41	0.24

mineralization in Gaudeanmus area, the Nd isotopic characteristics were determined for uraninites from the uraniferous leucogranites. Analytical results for the Sm-Nd study are presented in Table 5, showing a clustering of $(^{143}Nd/^{144}Nd)_i$ ratios at about 0.511147–0.511231 and highly negative $\varepsilon_{Nd}(t)$ values of −14.8 to −16.5.

In the $\varepsilon_{Nd}(t)$ vs t diagram (Fig. 7), evolution lines for the Etusis Formation, Khan Formation, and Kuiseb Formation were drawn based on the work of McDermott (1996). The evolution line for the Etusis Formation lies in the range of pre-Damara basement, indicating that strata of the Etusis Formation was mixed with a component of basement material, or was derived directly from the basement by erosion and subsequent deposition. The analyzed uraninite samples plot in the area of pre-Damara basement (Fig. 7).

6 Discussion

6.1 Petrogenesis of uraniferous leucogranites

At ca. 580 Ma, plate subduction led to convergence of the Kalahari and Congo cratons (Blaine, 1977; Sawyer, 1981), which resulted in continental collision between ca. 560 and 540 Ma (Kasch, 1983; Longridge et al., 2008). In the process of the collision which moulded the Damara Belt, the Damara sequence and basement rocks experienced multi-stage tectonic events, including the development of structural domes. The main structure of the intracontinental branch of the Damara Belt is NE-trending. The distinctive domes in the Central Zone is formed during the orogeny (Miller, 1979), which is also NE-trending. The collision also generated several phases of deformation, which is manifested as folds, faults, lineaments, and foliations.

Magmatism was active during the collision, resulting in several episodes of granitoid emplacement. The dioritic suite in the Goas area was dated at 563±4 Ma and 546±6 Ma (SHRIMP U-Pb zircon ages), representing the timing of plate subduction (Jacob et al., 2000). Subsequent syntectonic granites in the Gaudeanmus area, have yielded LA-ICP-MS U-Pb zircon ages of 552.5±2.2 Ma for a porphyritic granite and 540.2±3.9 Ma for a biotitic granite, both of which are similar to the Salem-type granites (Wang, 2013), indicating that the Kalahari and Congo cratons began to collide at ca. 560–540 Ma. B, C, and F-type leucogranites have LA-ICP-MS U-Pb zircon ages of 537.8±4.3 Ma, 525.4±2.6 Ma, and 511.4±4.3 Ma, respectively (Wang, 2013), indicating emplacement during the orogeny. In addition, deformation is dated at 520–508 Ma in the Central Zone (Jung, 2000; Longridge et al., 2011).

It is thought that collision of the Kalahari and Congo cratons had ceased by ca. 510–505 Ma, and the $^{40}Ar/^{39}Ar$

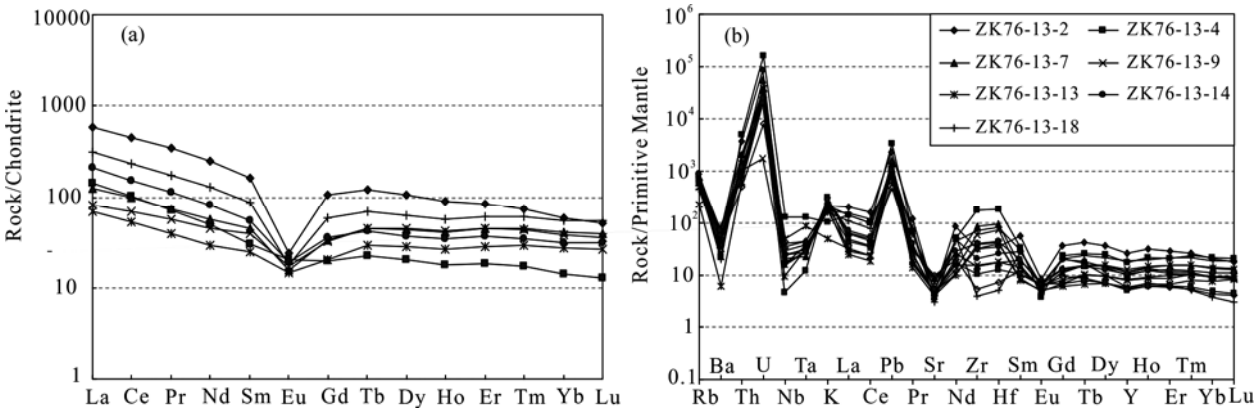

Fig. 5. (a) Chondrite-normalized REE patterns and (b) primitive-mantle normalized trace element spidergram for the uraniferous leucogranites in the Gaudeanmus area, Namibia (Sun and McDonough, 1989).

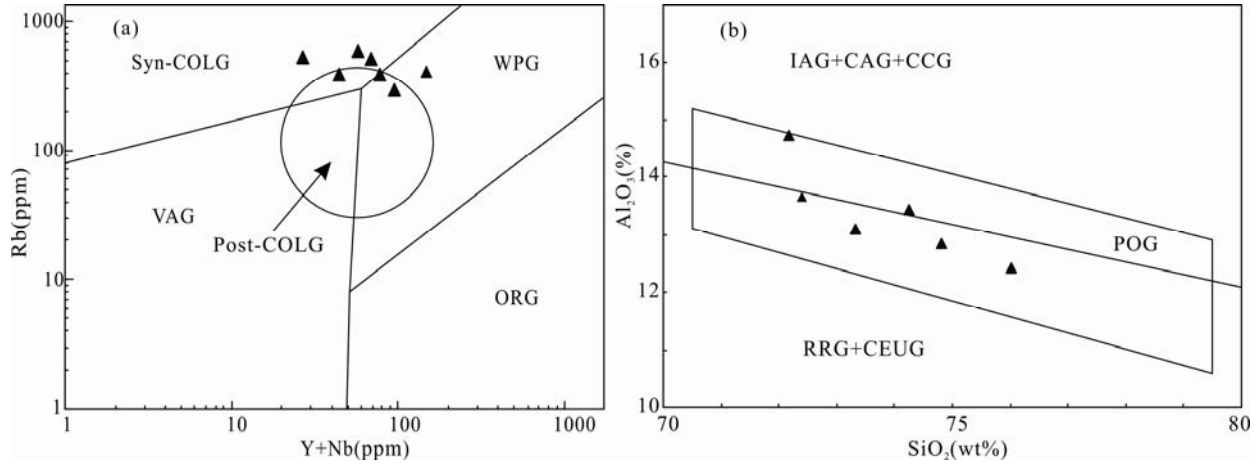

Fig. 6. (a) Rb vs Y+Nb diagram and (b) Al_2O_3 vs SiO_2 diagram for uraniferous leucogranites in the Gaudeanmus area, Namibia. VAG = volcanic arc granite; WPG = within plate granite; Post-COLG = post-collision granite; Syn-COLG = syn-collision granite; ORG = ocean ridge granite; IAG = island arc granite; CAG = continental arc granite; CCG = continental collision granite; POG = post orogenic granite; RRG = rift related granite; CEUG = continental epeirogenic uplifted granite.

Table 5 Sm-Nd isotopic compositions of uraninites in uraniferous leucogranites in the Gaudeanmus area, Namibia

Sample no.	Sm (ppm)	Nd (ppm)	$^{147}Sm/^{144}Nd$	$^{143}Nd/^{144}Nd$	±2σ	$(^{143}Nd/^{144}Nd)_i$	$\varepsilon_{Nd}(t)$	t_{DM}(Ga)	t_{2DM}(Ga)
ZK76-13-2	1275	2040	0.3779	0.512411	11E-06	0.511168	-16.1	3.29	2.53
ZK76-13-8	318	518	0.3705	0.512376	7E-06	0.511158	-16.3	3.04	2.55
ZK76-13-10	1332	2131	0.3778	0.512402	5E-06	0.51116	-16.2	2.90	2.54
ZK76-13-12	1182	1990	0.359	0.512328	8E-06	0.511147	-16.5	4.16	2.56
ZK76-13-16	1059	1754	0.3651	0.5124	7E-06	0.511199	-15.5	3.77	2.48
LS-2	1789	2431	0.4448	0.512694	7E-06	0.511231	-14.8	2.30	2.43
ZK84-6-3	934	1453	0.3886	0.512464	8E-06	0.511186	-15.7	2.69	2.5

$\varepsilon_{Nd}(t)$ is calculated at t=502 Ma for uraninite (Chen, 2014), with $(^{143}Nd/^{144}Nd)_{CHUR}$=0.512638 (Goldstein et al. 1984); $(^{147}Sm/^{144}Nd)_{CHUR}$=0.1967 (Jacobsen and Wasserburg, 1980). t_{2DM} is calculated using $(^{147}Sm/^{144}Nd)_{DM}$=0.2136, $(^{143}Nd/^{144}Nd)_{DM}$=0.51351 (Liew and Hofmann, 1988).

age of mica schist in the Damara Belt is 459±4 Ma, indicating that magmatism had stopped and the region had cooled below about 350℃ by 460 Ma (Gray et al., 2006). Two uraniferous leucogranites (i.e. D-type leucogranites) have yielded LA-ICP-MS U-Pb ages of 497±5.5 Ma (zircon; Wang, 2013) and 509±1 Ma (U-Pb monazite; Briqueu et al., 1980) suggesting emplacement in a post-orogenic environment. It has previously been noted that the known uranium deposits/occurrences in the southern Central Zone (i.e. Rössing, Valencia, Rössing South, Ida Dome, Goanikontes and Gaudeanmus area) all occur at or near the margins of the NE-NNE trending domes (Fig. 2), and especially along zones of curvature in the domal pattern (Corner, 1983; Anderson et al., 1997; Basson et al., 2004; Kinnaird et al., 2007). Formation of the domes would have been accompanied by the development of joints, fractures, and accommodation space in extensional settings. This not only would have provided space for the uraniferous leucogranite intrusions, but also would have facilitated uranium precipitation and enrichment. In

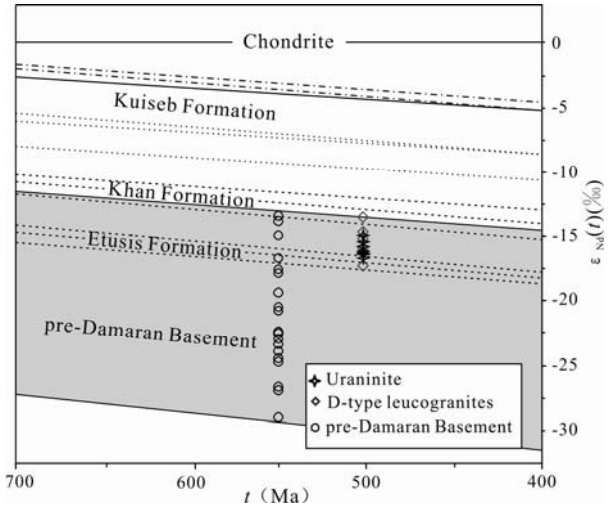

Fig. 7. εNd(t) vs t diagram for uraninites and uraniferous leucogranites in the Gaudeanmus area, Namibia.
Data for the pre-Damara basement are from Chen (2014), Seth et al. (2002), Kröner et al. (2004), and Janoušek et al. (2010); data for the uraniferous leucogranites are from Chen (2014);, and uraninite data are from this study.

addition to the spatial association with the margins of structural domes, most of the uranium deposits are located along, or proximal to (on both sides), the Welwitschia Lineament (Fig. 2), which is a NNE trending regional fault, implying a strong structural control on uranium mineralization. The fault responsible for the Welwitschia lineament induced secondary faults, joints, and schistosities, which helped provide conduits for ascending magma and accommodation space for intrusion emplacement. Intrusion of the uraniferous leucogranites took place after formation of the structural domes, indirectly supporting a post-orogenic origin.

According to the Rb-Y+Nb and SiO_2-Al_2O_3 diagrams (Fig. 6), the uraniferous leucogranites were formed in a post-orogenic extensional setting. Based on their trace-element signature (depleted Ba, Nb, Ta, Sr), their REE distribution, together with Sm-Nd results, the uraniferous leucogranites are interpreted as being derived by partial melting of upper-crustal source material.

6.2 Sources of uranium

The $(^{87}Sr/^{86}Sr)_i$ ratios of the uraniferous leucogranites are relatively high with a wide range of 0.73035–0.79345 (Chen, 2014). Due to the high Rb/Sr ratios of the uraniferous leucogranites, it is possible that a slight disturbance to the Rb-Sr isotopic system could have influenced the initial $^{87}Sr/^{86}Sr$ values; alternatively, the Rb/Sr system may not have remained closed as a result of post-orogenic geological events (Wu et al., 2002; Ling et al., 2006). However, The $(^{87}Sr/^{86}Sr)_i$ ratios of the uraniferous leucogranites are still within the range of the pre-Damara basement ($(^{87}Sr/^{86}Sr)_i$ = 0.70625 to 0.81824), thus it was interpreted as melts of the pre-Damara basement (Chen, 2014).

The Sm-Nd isotopic system is much more stable, and thus its use as a tracer to determine the source rocks of the uraniferous leucogranites is better than the Rb-Sr system. $(^{143}Nd/^{144}Nd)_i$ ratios of pre-Damara basement and the uraniferous leucogranites range from 0.510771–0.511163, and 0.511102–0.511301, respectively (Chen, 2014). In the $\varepsilon_{Nd}(t)$ - t diagram, the uraniferous leucogranites overlap the evolution fields defined by the Etusis Formation and pre-Damara basement (Fig. 7). Although the Etusis Formation itself was also derived from the pre-Damara basement, its U content is 2.42–3.36 ppm (average of 2.97 ppm). Due to the heterogeneity of the pre-Damara basement (Nex et al., 2001), the U content of uranium-rich part is 11.50–18.40 ppm (average of 14.63 ppm) (Chen, 2014), so the Etusis Formation was likely derived from the low uranium basement. It is therefore inferred that the uraniferous leucogranites mainly originated from the pre-Damara basement. Moreover, the uraninite also plot in the area of pre-Damara basement (Fig. 7), suggesting that the magmatic component of the ore came from the same uranium-rich, pre-Damara basement.

Nd model ages may also help to constrain the source of the uranium and uraniferous leucogranites (Qi et al., 2007; Zhang et al., 2007; Jahn et al., 2013). The uraninites yield two-stage Nd model ages of 2.43–2.56 Ga, which is also the approximate age of two-stage Nd model ages of the pre-Damara basement (2.26–3.32 Ga) (Janoušek et al., 2010), suggesting that that the uranium-rich, pre-Damara basement was the main source of the main magmatic component of the uranium mineralization.

Based on uranium mineralogy, the subsequent hydrothermal component of uranium mineralization may have resulted from remobilization. The pitchblende and veinlet-shaped coffinite are generally spatially related to the uraninite, uranothorite, euhedral coffinite, pyrite, and chlorite, or in fractures within them (Fig. 3c). It is therefore inferred that pitchblende and veinlet-shaped coffinite were formed by hydrothermal remobilization of uranium from uranium minerals that crystallized during the main magmatic component of mineralization. Precipitation is attributed to reducing reactions with sulphide minerals and generally took place in close proximity to the primary igneous minerals.

7 Conclusions

Uraniferous leucogranites of the Gaudeanmus area are subalkaline and metaluminous to weakly peraluminous rocks. They possess high silica (68.81wt%–76.02wt%, average 73.11wt%) and total alkali (K_2O+Na_2O 8.51wt%–

11.79wt%, average 9.66wt%) concentrations, are enriched in potassium and depleted in MnO, TiO_2, and MgO, and have A/CNK ratios of 0.96–1.07 (average of 1.01). Total REE concentrations range from 96.54 ppm to 695.24 ppm, averaging 264.37 ppm, with higher concentrations of LREE (LREE/HREE=2.53–7.71, average 5.03; $(La/Yb)_N$=2.14–10.40, average 5.85), and moderate Eu depletion (δEu=0.18–0.80, averagely 0.45). The leucogranites have high Rb/Sr ratios (2.03–5.50, with an average of 4.36), with enriched Rb, Th, U, K, and Pb, and depleted Ba, Nb, Ta, and Sr. Based on the trace-element signature, REE distribution and Sm-Nd results, the uraniferous leucogranites were formed in a post-orogenic extensional setting and was derived from partial melting of the U-rich pre-Damara basement.

Uraninites show highly negative $\varepsilon_{Nd}(t)$ values of −14.8 to −16.5 and $(^{143}Nd/^{144}Nd)_i$ ratios of 0.511147–0.511231. Two-stage Nd model ages for the pitchblende range from 2.43 to 2.56 Ga, which is similar to the two-stage Nd model ages of pre-Damara basement (2.26–3.32 Ga), and derived $\varepsilon_{Nd}(t)$ values lie within the range of pre-Damara basement. All these lines of evidence suggest that the magma-derived uranium emplaced during the main mineralization event in the Gaudeanmus area mainly came from the uranium-rich pre-Damara basement. This was overprinted by a subsequent hydrothermal event during which uranium was remobilized from the magma-derived minerals and precipitated as pitchblende and coffinite.

Acknowledgements

We are most grateful to AGS reviewers Hongfei Ling and Kenneth Ashton as well as Associate Editor Guoxiang Chi for critical and constructive comments that greatly improved the manuscript. We also appreciate Professor Jiashu Rong from Beijing Research Institute of Uranium Geology for many fruitful discussions and suggestions. This study was supported by the National Natural Science Foundation of China (41602080) and Nuclear Energy Development Project from the National Defense Science and Industry Bureau.

Manuscript received July. 1, 2016
accepted Aug. 1, 2017
edited by Liu Lian

References

Anderson, H., and Nash C., 1997. Integrated lithostructural mapping of the Rössing area, Namibia using high resolution aeromagnetic, radiometric Landsat data and aerial photographs. *Exploration Geophysics*, 28(2): 185–191.

Barnes, J.F.H., and Hambleton-Jones, B.B., 1978. A review of the geological and geochemical setting of uraniferous granites in the Damara Orogen. *Lecture to the IAEA working group meeting, Nancy, France, Report GEA 525, Pelindaba*, Nuclear Development Corporation of South Africa.

Basson, I.J., and Greenway, G., 2004. The Rössing uranium deposit: a product of late-kinematic localization of uraniferous granites in the Central Zone of the Damara Orogen, Namibia. *Journal of African Earth Sciences*, 38(5): 413–435.

Blaine, J.L., 1997. Tectonic evolution of the Waldau Ridge structure and the Okahandja Lineament, South West Africa. *Precambrian Research Unit Bulletin*, 21.

Briqueu, L., Lancelot, J.R., Valois, J.P., and Walgenwitz, F., 1980. "Géochronologie U-Pb et genèse d'un type de minéralisation uranifère: les alaskites de Goanikontès (Namibie) et leur encaissant', *Bull. Centre Rech. Explor. Prod. Elf. Aquitaine*, 4: 759–811.

Brynard, H.J., and Andreoli, M.A.G., 1988. An overview of the regional geological and structural setting of the uraniferous granites in the Damara Orogen, Namibia. In: *IAEA Proceedings of a Technical Committee Meeting on Recognition of Uranium Provinces, IAEA, Vienna*, pp. 195–212.

Chen Jinyong, 2014. *The Mineralization Mechanism Study of Leucogranite-type Uranium Deposite around Gaudeanmus, Namibia*. Beijing: Beijing Research Institute of Uranium Geology (Ph.D thesis): 1–179.

Chen Jinyong, Fan Honghai, Chen Donghuan, Gu Dazhao and Wang Shengyun, 2013. Research on the Characteristics of Uranium Minerals of Alaskite-type Uranium Deposit in the Gaudeanmus Area, Namibia. *Geological Review,* 59(5): 962–970 (in Chinese with English abstract).

Chen Jinyong, Fan Honghai, Chen Donghuan, Gu Dazhao and Wang Shengyun, 2014. Texture and Structure of Ore and Genesis of Alaskite-type Uranium Deposit in the Gaudeanmus Area, Namibia. *Bulletin of Mineralogy, Petrology and Geochemistry*, 33(1): 91–97 (in Chinese with English abstract).

Corner, B., 1983. An interpretation of the aeromagnetic data covering the western portion of the Damara Orogen in South West Africa/ Namibia. *Special Publication of the Geological Society of South Africa*, 11: 339–354.

Corner, B., Henthorn, D.I., 1978. Results of a palaeomagnetic survey undertaken in the Damara mobile belt, South West Africa, with special reference to the magnetisation of the uraniferous pegmatitic granites. *Report PEL-260 Pelindaba, Atomic Energy Board South Africa*.

Corvino, A.F., and Pretorius, L.E., 2013. Uraniferous leucogranites south of Ida Dome, central Damara Belt, Namibia: Morphology, distribution and mineralization. *Journal of African Earth Sciences*, 80(4): 60–73.

Coward, M. P., 1983. The tectonic history of the Damara Belt. In: Miller, R. McG. (ed.), *Evolution of the Damara Orogen of South West Africa/Namibia*. Geological Society of South Africa, Special Publication, 409–421.

Cuney, M., 1980a. Petrography geochemistry and fluid inclusion studies of the Rössing alaskites and surrounding gneisses. *Nancy, Centre de Recherches sur la Geologie de l'uranium*, 58.

Cuney, M., 1980b. Preliminary results on the petrology and fluid inclusions studies of the Rössing uraniferous alaskites. *Transactions of the Geological Society of South Africa*, 83: 39–45.

De Flierdt, T.V., Hoernes, S., Jung, S., Masberg, P., Hoffer, E., Schaltegger, U., Friedrichsen, H., 2003. Lower crustal melting and the role of open-system processes in the genesis of syn-orogenic quartz diorite–granite–leucogranite associations: constraints from Sr–Nd–O isotopes from the Bandombaai Complex, Namibia. *Lithos*, 67(3–4): 205–226.

Ding Chengwu, Dai Pan, Bagas Leon, Nie fengjun, Jiang Sihong, Wei Junhao, Ding Chengzhen, Zuo Pengfei and Zhang Ke, 2016. Geochemistry and Sr-Nd-Pb Isotopes of the Granites from the Hashitu Mo Deposit of Inner Mongolia, China: Constraints on Their Origin and Tectonic Setting. *Acta Geologica Sinica* (English Edition), 90(1): 106–120.

Fan Honghai, Chen Jinyong, Gu Dazhao and Wang Shengyun, 2015. The fluid inclusions and metallogenesis of alaskite-type uranium deposit in the Gaudeanmus area, Namibia. *Mineral Deposits*, 34(1): 189–199 (in Chinese with English abstract).

Freemantle, G.G., 2010. *Petrographic, Mineralogical and Geochemical Characterisation of Granite-hosted Uranium Deposits of the Central Damara Orogen, Namibia*. South Africa: University of the Witwatersrand Johannesburg (unpublished Ph.D. Thesis).

Gao, J.F., Lu, J.J., Lai, M.Y., Lin, Y.P., and Pu W., 2003. Analysis of trace elements in rock samples using HR-ICP-MS. *Journal of Nanjing University Natural Sciences,* 39: 844–850.

Goldstein, S.L., O'Nions R.K., and Hamilton P.J., 1984. A Sm-Nd isotopic study of atmospheric dusts and particulates from major river systems. *Earth & Planetary Science Letters*, 70 (2): 221–236.

Gray, D.R., Foster, D.A., Goscombe, B., Passchier, C.W., Trouw, R.A.J., 2006. $^{40}Ar/^{39}Ar$ thermochronology of the Pan-African Damara Orogen, Namibia, with implications for tectonothermal and geodynamic evolution. *Precambrian Research*, 150(1–2): 49–72.

Haack, U., Gohn, E., Hartmann, O., 1983. Radiogenic heat generation in Damaran rocks. In: Miller, R.McG (Ed.), *Evolution of the Damara Orogen of South West Africa/ Namibia*. Geological Society of South Africa, Special Publication, 11: 225–232.

Hoffmann, K.H., Condon, D.J., Bowring, S.A., and Crowley, J.L., 2004. U-Pb zircon date from the Neoproterzoic Ghaub Formation, Namibia: Constraints on Marinoan glaciations. *Geology*, 32(9): 817–820.

Hoffmann, K.H., Hawkins, D.P., Isachsen, C.E., and Bowring, S.A., 1996. Precise U-Pb zircon ages for early Damaran magmatism in the Summas Mountains and Welwitschiainlier, northern Damara belt, Namibia. *Communications Geological Survey of Namibia*, 11: 47–52.

Irvine, T.N., and Baragar, W.R.A., 1971. A guide to the chemical classification of the common volcanic rocks. *Canadian Journal of Earth Sciences*, 8(5): 523–548.

Jacob, R.E., Kröner, A., and Burger, A.J., 1978. Areal extent and first U-Pb age of Pre-Damaran Abbabis Complex in the Central Damaran belt of South West Africa. *Geologische Rundschau,* 67(2): 706–718.

Jacob, R.E., Moore, J.M., Armstrong, R.A., 2000. SHRIMP dating and implications of Au mineralization, Navachab, Namibia. Abstracts, Geological Society of South Africa Geocongress 2000: A New Millennium on Ancient Crust. *Journal of African Earth Sciences*, 31: 32–33.

Jacobsen, S.B., and Wasserburg, G.J., 1980. Sm-Nd isotopic evolution of chondrites. *Earth & Planetary Science Letters*, 50 (1):139–155

Jahn B., Usuki M., Ishihara S., Okamoto K., and Usuki T., 2013. Accretionary Orogens of the Japanese Islands and Their Comparison with the Central Asian Orogenic Belt: Sr-Nd-Hf Isotopic Evidence. *Acta Geologica Sinica* (English Edition), 87(supp.): 302–304.

Janoušek, V., Konopásek, J., Ulrich, S., Erban, V., Tajčmanová, L., and Jeřábek, P., 2010. Geochemical character and petrogenesis of Pan-African Amspoort suite of the Boundary Igneous Complex in the Kaoko Belt (NW Namibia). *Gondwana Research*, 18(4): 688–707.

Jung, S., 2000. High-temperature, low/medium-pressure clockwise P-T paths and melting in the development of regional migmatites: the role of crustal thickening and repeated plutonism. *Geological Journal*, 35(3–4): 345–359.

Kasch, K.W., 1983. Folding and thrust tectonics in the south-eastern portion of the Damara Orogen around Omitara, Namibia. In: Miller, R. McG. (Ed.), *Evolution of the Damara Orogen of South West Africa/Namibia*. Geological Society of South Africa, Special Publication, 11: 175–184.

Kinnaird, J.A., and Nex, P.A.M., 2007. A review of geological controls on uranium mineralization in sheeted leucogranites within the Damaran Orogen, Namibia. *Applied Earth Science* (Trans. Inst. Min. Metall. B), 116(2): 68–85.

Kitt, S., 2008. *Structural controls of auriferous quartz veins in the Karibib area, southern central zone of the Pan-African Damara belt, Namibia*. South Africa: University of Stellenbosch (MSc. Thesis): 1–133.

Kröner, S., Konopásek, J., Kröner, A., Passchier, C.W., Poller, U., Wingate, M.T.D., Hofmann, K.H., 2004. U-Pb and Pb-Pb zircon ages for metamorphic rocks in the Kaoko Belt of northwestern Namibia: a Palaeo- to Mesoproterozoic basement reworked during the Pan-African orogeny. *South African Journal of Geology*, 107(3): 455–476.

Liew, T.C., and Hofmann, A.W., 1988. Precambrian crust components, plutonic associations, plate environment of the Hercynian Fold Belt of central Europe: Indication from Nd and Sr study. *Contributions to Mineralogy & Petrology*, 98(2): 129–138.

Ling Hongfei, Shen Weizhou, Sun Tao, Jiang Shaoyong, Jiang Yaohui, Ni Pei, Gao Jianfeng, Huang Guolong, Ye Haimin and Tan Zhengzhong, 2006. Genesis and source characteristics of 22 Yanshanian granites in Guangdong province: study of element and Nd-Sr isotopes. *Acta Petrologica Sinica*, 22(11): 2687–2703 (in Chinese with English abstract).

Longridge. L., Gibson, R.L., Kinnaird, J.A., and Armstrong, R.A., 2011. Constraining the timing of deformation in the southwestern Central Zone of the Damara Belt, Namibia. *Geological Society, London, Special Publications*, 357(1): 107 –135.

Longridge, L., Gibson, R.L., Kinnaird, J.A., and Armstrong, R.A., 2008. *Timing of deformation and granite emplacement in the Central Zone of the Damara Orogen, Namibia*. School of Geosciences, University of the Witwatersrand Johannesburg (Unpublished report).

Maniar, P.D., and Piccoli, P.M., 1989. Tectonic discrimination of granitoids. *Geological Society America Bulletin*, 101(5): 635–643.

Martin, H., and Porada, H., 1977. The intracratonic branch of the Damaran Orogen in Namibia. Discussion of geodynamic

models. *Precambrian Research*, 5(4): 311–338.

McDermott, F., Harris, N.B.W., and Hawkesworth, C.J., 1996. Geochemical constraints on crustal anatexis: a case study from the Pan-African Damara granitoids of Namibia. *Contributions to Mineralogy and Petrology*, 123(4): 406–423.

Miller, R. McG., 1979. The Okahandja Lineament, a fundamental tectonic boundary in the Damara Orogen of South West Africa/Namibia. *Transactions of the Geological Society of South Africa*, 82: 349–361.

Miller, R. McG., 1983. The Pan-African Damara Orogen of South West Africa/Namibia. In: Miller, R. McG. (ed.), *Evolution of the Damara Orogen of South West Africa/ Namibia*. Geological Society of South Africa, Special Publications, 11: 431–515.

Nex, P.A.M., 1997. *Tectono-metamorphic setting and evolution of granitic sheets in the Goanikontes area, Namibia*. Galway: National University of Ireland (Ph.D. Thesis):1–155.

Nex, P.A.M., Herd, D., and Kinnaird, J.A., 2002. Fluid extraction from quartz in sheeted leucogranites as a monitor to styles of uranium mineralisation: an example from the Rössing area, Namibia. *Geochemistry: Exploration, Environment, Analysis*, 2(1): 83–96.

Nex, P.A.M., Kinnaird, J.A., and Oliver, G.J.H., 2001. Petrology, geochemistry and uranium mineralisation of post collisional magmatism around Goanikontes, southern Central Zone, Namibia. *Journal of African Earth Sciences*, 33(3): 481–502.

Pearce, J.A., 1996. Sources and setting of granitic rocks. *Episodes*, 19(4): 120–125.

Qi Changshi, Deng Xiguang, Li Wuxian, Li Xianhua, Yang Yueheng and Xie Liewen, 2007. Origin of the Darongshan-Shiwandashan S-type granitoid belt from southeastern Gangxi: Geochemical and Sr-Nd-Hf isotopic constraints. *Acta Petrologica Sinica*, 23(2): 403–412 (in Chinese with English abstract).

Roesener, H., and Schreuder, C.P., 1994. 'Nuclear and Fossil Fuels-Uranium' in *Mineral Resources of Namibia*. Ch. 7.1, p. 1–59.

Sawyer, E.W., 1981. Damaran structural and metamorphic geology of an area south-east of Walvis Bay, South West Africa/Namibia. *Geological Survey of South West Africa/ Namibia*, 7: 94.

Seth, B., Jung, S., and Hoernes, S., 2002. Isotope constraints on the origin of Pan-African granitoid rocks in the Kaoko belt, NW Namibia. *South African Journal of Geology*, 105(2): 179–192.

Seth, B., Kröner, A., Mezger, K., Nemchin, A.A., Pidgeon, R.T., and Okrusch, M., 1998. Archaean to Neoproterozoic magmatic events in the Kaoko Belt ofNWNamibia and their geodynamic significance. *Precambrian Research*, 92(4): 341–363.

Smith, D.A.M., 1965. The geology of the area around the Khan and Swakop Rivers in South West Africa. *Memoir of the Geological Survey of South Africa*, 1: 113.

Sun, S.S., and McDonough, W.F., 1989. Chemical and isotopic systematic of oceanic basalts: Implications for mantle composition and processes. Saunders A D and Norry M J. Magmatism in Oceanic Basins. *Geological Society London Special Publications*, 42 (1): 313–345.

Taylor, S.R., and McLennan, S.M., 1995. The geochemical evolution of the continental crust. *Reviews of Geophysics*, 33 (2): 293–301.

Wang Shengyun, 2013. *Petrology, geochemistry and genesis of Granitoids in the Gaudeanmus Area, Namibia*. Beijing: Beijing Research Institute of Uranium Geology (Ph.D thesis): 1–177.

Wu F.Y., Sun D.Y., Li H.M., Jahn B.M., and Wilde, S., 2002. A-type granites in northeastern China: age and geochemical constraints on their petrogenesis. *Chemical Geology*, 187(1–2): 143–173.

Zhang Guicun, Cui Jianyong and Gao Dingshun, 1999. *Analytical Methods for Pb, Sr, Nd isotopes in Rocks*. Beijing: Standards Press of China.

Zhang Hongfei, Jin Lanlan, Zhang Li, Nigel Harris, Zhou Lian, Hu Shenghong and Zhang Benren, 2007. Geochemical and Pb -Sr-Nd isotopic compositions of granitoids from western Qinling belt: Constraints on basement nature and tectonic affinity. *Science in China Series D: Earth Sciences*, 50(2): 184 –196.

Zhang Xiangxin, Su Zhen and Gao Yongfeng, 2017. Zircon U-Pb Geochronology and Geochemistry of the Early Cretaceous Volcanic Rocks from the Manitu Formation in the Hongol Area, Northeastern Inner Mongolia. *Acta Geologica Sinica* (English Edition), 91(4): 1286-1304.

Zong Keqing, Chen Jinyong, Hu Zhaochu, Liu Yongsheng, Li Ming, Fan Honghai and Meng Yanning, 2015. In-situ U-Pb dating of uraninite by fs-LA-ICP-MS. *Science China: Earth Sciences*, 58(10): 1731–1740.

About the first author

FAN Honghai, born in 1963, professor and doctoral supervisor. He got his PH. D in Nanjing University. Currently he is engaged in the study of Uranium geology. E-mail: fhh270@263.net.